Journal of Ginseng Research 47 (2023) 743–754

Contents lists available at ScienceDirect

Journal of Ginseng Research

journal homepage: https://www.sciencedirect.com/journal/journal-of-ginseng-research

Research Article

20(S)-ginsenoside Rg3 exerts anti-fibrotic effect after myocardial infarction by alleviation of fibroblasts proliferation and collagen deposition through TGFBR1 signaling pathways

Honglin Xu [a, b, c, 1], Haifeng Miao [a, 1], Guanghong Chen [b, c], Guoyong Zhang [b, c], Yue Hua [b, c], Yuting Wu [b, c], Tong Xu [b, c], Xin Han [b, c], Changlei Hu [b, c], Mingjie Pang [b, c], Leyi Tan [d], Bin Liu [e, **], Yingchun Zhou [a, b, c, *]

[a] Department of Geratology, Affiliated Dongguan Hospital, Southern Medical University (Dongguan People's Hospital), Dongguan, China
[b] School of Traditional Chinese Medicine, Southern Medical University, Guangzhou, China
[c] Department of Traditional Chinese Medicine, Nanfang Hospital (ZengCheng Branch), Southern Medical University, Guangzhou, China
[d] The First School of Clinical Medicine, Southern Medical University, Guangzhou, China
[e] Department of Traditional Chinese Medicine, the Second Affiliated Hospital of Guangzhou Medical University, Guangzhou, China

ARTICLE INFO

Article history:
Received 17 January 2023
Received in revised form
23 June 2023
Accepted 24 June 2023
Available online 03 July 2023

Keywords:
CFs proliferation
Collagen deposition
Myocardial fibrosis post myocardial infarction
TGFBR1
20(S)-ginsenoside Rg3

ABSTRACT

Background: Myocardial fibrosis post-myocardial infarction (MI) can induce maladaptive cardiac remodeling as well as heart failure. Although 20(S)-ginsenoside Rg3 (Rg3) has been applied to cardiovascular diseases, its efficacy and specific molecular mechanism in myocardial fibrosis are largely unknown. Herein, we aimed to explore whether TGFBR1 signaling was involved in Rg3's anti-fibrotic effect post-MI.

Methods: Left anterior descending (LAD) coronary artery ligation-induced MI mice and TGF-β1-stimulated primary cardiac fibroblasts (CFs) were adopted. Echocardiography, hematoxlin-eosin and Masson staining, Western-blot and immunohistochemistry, CCK8 and Edu were used to study the effects of Rg3 on myocardial fibrosis and TGFBR1 signaling. The combination mechanism of Rg3 and TGFBR1 was explored by surface plasmon resonance imaging (SPRi). Moreover, myocardial *Tgfbr1*-deficient mice and TGFBR1 adenovirus were adopted to confirm the pharmacological mechanism of Rg3.

Results: *In vivo* experiments, Rg3 ameliorated myocardial fibrosis and hypertrophy and enhanced cardiac function. Rg3-TGFBR1 had the 1.78×10^{-7} M equilibrium dissociation constant based on SPRi analysis, and Rg3 inhibited the activation of TGFBR1/Smads signaling dose-dependently. Cardiac-specific *Tgfbr1* knockdown abolished Rg3's protection against myocardial fibrosis post-MI. In addition, Rg3 down-regulated the TGF-β1-mediated CFs growth together with collagen production *in vitro* through TGFBR1 signaling. Moreover, TGFBR1 adenovirus partially blocked the inhibitory effect of Rg3.

Conclusion: Rg3 improves myocardial fibrosis and cardiac function through suppressing CFs proliferation along with collagen deposition by inactivation of TGFBR1 pathway.

1. Introduction

Cardiovascular diseases (CVDs), which mainly include stroke and ischemic heart disease (IHD), have been identified as the major factor inducing death worldwide [1], and IHD was found to account for 49.2% in 2019 [2]. Acute myocardial infarction (MI) is characterized by the massive loss of cardiomyocytes resulting from a dramatic decrease in coronary blood flow. As a consequence, fibroblasts are activated to produce the reparative extracellular matrix (ECM) for maintaining structural integrity and preventing sudden ventricular rupture after infarction [3]. However, excessive

* Corresponding author. Affiliated Dongguan Hospital, Southern Medical University (Dongguan People's Hospital), Dongguan, 523058, China.
** Corresponding author.
E-mail addresses: xmhoolv@163.com (B. Liu), zhychun@126.com (Y. Zhou).
[1] Equal contribution in the manuscript.

https://doi.org/10.1016/j.jgr.2023.06.007

collagen sediment will disrupt the myocardial systolic and diastolic functions, ultimately inducing maladaptive ventricular remodeling and heart failure (HF) [4]. Although the mortality apparently declines thanks to the availability of reperfusion therapy techniques at present, there are still many patients entering the rehabilitation phase post-MI and suffering from myocardial fibrosis. Therefore, inhibition of immoderate myocardial fibrosis can effectively protect patients' cardiac function and improve their prognosis. Moreover, it is extremely urgent to develop new pharmacological therapeutics to inhibit the unrestricted ECM and collagen deposition.

Ginsenoside Rg3, a natural triterpenoid saponin of traditional Chinese medicine (TCM) *Panax ginseng* Meyer, has been suggested to exert numerous biological activities, such as anti-bacteria, anti-tumor, anti-inflammation, antioxidation, and anti-apoptosis [5–8]. There are S and R optical isomers of ginsenoside Rg3 depending on the spatial arrangement of the hydroxyl radical at carbon-20 [9]. The isomers exhibit different physical properties and biological activities, and 20(S) isomer has a much higher solubility and more bioavailable than 20(R) [10]. Recently, the therapeutic applications of 20(S)-ginsenoside Rg3 (Rg3) in CVDs have attracted increasing attention [11]. Other basic studies have shown that Rg3 attenuates myocardial hypertrophy mediated by the transverse aortic constriction in rats [12], while Rg3 attenuates myocardial dysfunction and collagen deposition in HF mice by targeting the metabolic degradation enzyme aminoglycosidase-1 [13]. However, the role of Rg3 in regulating adverse ventricular remodeling after infarction remains largely unclear, and the underlying molecular mechanism of Rg3 in myocardial fibrosis has not yet been fully elucidated, which deserves more investigations.

Transforming growth factor-β (TGF-β) family is closely correlated with fibrotic processes in multiple organs (like heart, liver, and kidney). In canonical TGF-β signaling, TGF-β1 binds to TGF-β receptor I (TGFBR1), a kinase also known as ALK5, thus initiating and phosphorylating its downstream signaling molecules Smad2 and Smad3 [14]. Subsequently, a complex composed of Smad2/Smad3 and Smad4 trans-locates into the nucleus to up-regulate the expression of fibro-genic factors [14]. After activation of TGFBR1 signaling, cardiac fibroblasts (CFs) proliferate profusely and massive extracellular collagen is deposited in ischemic myocardium. These pathological changes will cause myocardial fibrosis and maladaptive ventricular remodeling, ultimately leading to HF [15]. Targeting TGFBR1 signaling pathway may be an effective treatment for mitigating reactive fibrosis and cardiac remodeling. Previous clinical trials adopt TGFBR1 inhibitors for the treatment of multiple diseases [16,17]. Nevertheless, up to now, no TGFBR1 inhibitor has been approved for clinical application due to its unfavorable characteristics like severe adverse effects, insignificant and individualized efficacy [18]. Therefore, it is significant to explore the efficient and safe novel TGFBR1 inhibitors to treat myocardial fibrosis post-infarction.

There is no evidence about whether Rg3 reduces fibroblasts proliferation as well as collagen deposition in TGF-β1-stimulated primary CFs and alleviates myocardial fibrosis in MI mice by targeting TGFBR1. More importantly, it is essential to comprehensively elucidate the regulatory mechanisms of Rg3 in CVDs from a new perspective. In the current study, the MI mouse modeling was performed through ligating left anterior descending (LAD) coronary artery to assess the therapeutic role of Rg3. Besides, mice with myocardial *Tgfbr1* deletion were adopted for verifying the Rg3-related mechanism. Moreover, Rg3's *in-vitro* inhibition of TGF-β1-stimulated CFs growth together with collagen deposition was assessed, then its pharmacological mechanism was confirmed by using TGFBR1 adenovirus.

2. Materials and methods

2.1. Materials

Rg3, molecular formula $C_{42}H_{72}O_{13}$ and molecular weight 785.01 g/mol, was purchased from Chengdu Must Biotechnology (Chengdu, China). The ^{1}H- and ^{13}C-NMR spectra of Rg3 were provided in Supplementary Fig. S1, which were similar to those reported for 20(S) isomer of ginsenoside Rg3 [19]. Its purity was determined by HPLC (purity, 98.2%; Supplementary Fig. S2). Captopril (Cap) was purchased from Solarbio (Beijing, China). Our work obtained antibodies targeting p-TGFBR1 (Ser165, #AF8080), TGFBR1 (#AF5347), p-Smad2 (Ser465+Ser467, #AF8314), Smad2 (AF6449), p-Smad3 (Ser423+Ser425, #AF8315), Smad3 (#AF6362), and GAPDH in Affinity Biosciences (Cincinnati, OH, USA), whereas those targeting PCNA (#A5324), CDK6 (#A5129), and Cyclin D1 (#A5035) in Bimake (Houston, TX, USA). The collagen I (#YT6057) and collagen III (#YM3123) were provided by ImmunoWay (Plano, TX, USA).

2.2. Animal experiments

The 6-8-week-old male C57BL/6, *Tgfbr1*$^{flox/flox}$ (Jackson Laboratories, #028701, Bar Harbor, ME, USA), and MCK-Cre mice (Jackson Laboratories) were kept in the specific pathogen-free environment. *Tgfbr1*$^{flox/flox}$ and MCK-Cre mice were utilized to generate cardiac-specific conditional *Tgfbr1* knockout mice (*Tgfbr1*$^{\Delta MCK}$). Each animal experimental procedure gained approval from Ethics Committee of Southern Medical University, and the methodology in the present work was performed according to specific instructions.

The LAD coronary artery was ligated to build the MI model according to previous description [20]. Briefly, 50 mg/kg pentobarbital sodium was injected into adult male mice for anesthesia, and mice then breathed with assistance of ventilator before surgical operation. A 2-3 cm skin incision was made in the third and fourth intercostal muscle of left sternum, followed by layer-by-layer separation of subcutaneous tissue, muscle and pericardium for exposing the visual field of heart. Then, an 8-0 silk wire was used to ligate LAD coronary artery. Subsequently, this work randomized the surviving operation animals as 4 groups (n = 8), including model, Rg3 low-dose (20 mg/kg/d, ig), Rg3 high-dose (40 mg/kg/d, ig) and cap (20 mg/kg/d, ig) groups. For mice in the sham group, only subcutaneous tissue and muscle were separate, without ligation of LAD. For reverse validation experiments, *Tgfbr1*$^{\Delta MCK}$ mice and *Tgfbr1*$^{flox/flox}$ male mice were randomized as 3 groups (n = 7), including sham, model and Rg3 groups (40 mg/kg/d, ig). All animals were examined by echocardiography 4 weeks later, and their hearts were removed.

2.3. Echocardiography

First of all, 1.5% isoflurane was given into each mouse through intranasal administration for anesthesia. Subsequently, the Vevo2100 High-resolution echocardiography was utilized to observe heart activity at a probe frequency of 38 MHz. Besides, M-mode echocardiography in the parasternal long-axis view was conducted to measure left ventricular ejection fraction (LVEF), left ventricular end-diastolic diameter (LVDd), left ventricular end-systolic diameter (LVDs), along with fractional shortening (FS), and the averages of all parameters were calculated from 3 consecutive cardiac cycles.

2.4. Histological examination

After dissection of heart tissues, they were subject to PBS rinsing, 4% paraformaldehyde (PFA) fixation, gradient ethanol dehydration, xylene immersion, paraffin embedding, and slicing in the 4-μm sections. Myocardial morphology in mice was examined by hematoxylin-eosin (HE) staining, while collagen volume fraction was analyzed after Masson trichrome staining using ImageJ software.

2.5. Immunohistochemical (IHC) analysis

In IHC assay, xylene I/II/III were added to deparaffinize, followed by gradient ethanol dehydration. The antigen was repaired, and endogenous peroxidase blocker was added to reduce nonspecific staining, followed by 5% goat serum incubation. The monoclonal antibodies targeting p-TGFBR1 (1:50), p-Smad2 (1:50), and p-Smad3 (1:100) were incubated under 4°C overnight. On the following day, corresponding biotin-coupled secondary antibodies were added to incubate sections. Positive staining was visualized with DAB (DAB-0031, MXB Biotechnologies). An optical microscope (Nikon Eclipse Ti-S, Tokyo, Japan) was used to photograph at × 200 magnification. Positive staining analysis was performed by ImageJ software.

2.6. Surface plasmon resonance imaging (SPRi)

Kx5 S equipment (Plexera, USA) was performed to quantitatively probe binding mechanisms underlying TGFBR1 and Rg3 in a real-time manner. To be specific, Rg3 was diluted to 5, 10, and 20 μM circulating compound. After fixing recombinant human TGFBR1 protein (Sino Biological Inc., Beijing, China) on the biochip, different concentrations of Rg3 were loaded on the Kx5 S equipment in accordance with specific protocols. The characteristic Rg3-to-TGFBR1 protein binding curve included 300-s association, 300-s dissociation, as well as 200-s reconstruction. Any alteration of binding signal was converted into standard refractive units (RU) as described previously [21].

2.7. CFs isolation and culture

Briefly, hearts were harvested from 1-3-day-old Sprague–Dawley (SD) rats and immediately rinsed in the pre-cooled D-Hank's solution thrice, followed by 0.25% trypsin incubation under 4°C overnight. BSA (5 mg/ml) as well as type II collagenase (1 mg/ml) were added and heart tissues were digested under 15-min shaking at 300 r/min thrice. After centrifugation, cells were collected on the plates for 90 min to separate CFs from cardiomyocytes by means of differential adsorption. After removal of cardiomyocytes, fresh medium was added and CFs were further cultured with 5% CO_2 under 37°C.

2.8. Cell proliferation assay

The CCK8 assay was performed to analyze cell proliferation. In summary, CFs were collected at the logarithmic phase and placed (5×10^3/well) into the 96-well plates. Each group was exposed to 48-h corresponding treatment following 24-h serum starvation. CCK8 solutions were added, following by 1-h incubation under 37°C. At last, the OD value was detected using the microplate reader at 450 nm.

2.9. Edu assay

Cell-LightTM Edu Apollo® 488 *In Vitro* Imaging Kit (RiboBio, Guangzhou, China) was employed to examine how Rg3 affected CFs proliferation. Briefly, CFs (5×10^3/well) were inoculated into 96-well plates, followed by pretreatment using Rg3 at diverse doses and TGF-β1 (10 ng/ml, PeproTech, Rocky Hill, NJ, USA), and then incubation with Edu solution for 4 h. After 30-min fixation with 4% PFA, cells were added with 1 × Apollo® staining reaction solution for 30-min incubation. Finally, 1 × Hoechst 33342 was added into each well for 30-min nuclear staining. Later, Edu-positive cell proportion was calculated as Edu-stained cell number (red fluorescence)/Hoechst 33342-stained cell number (blue fluorescence) × 100%.

2.10. Western-blot (WB) assay

WB assay was carried out according to previous description [22]. In brief, RIPA buffer (Beyotime, Shanghai, China) was added and BCA protein assay kit (Beyotime) was utilized to detect total protein contents. Thereafter, 30-μg proteins were separated by 10% SDS-PAGE, followed by transfer onto PVDF membranes (Millipore, Bedford, MA, USA). Then, 5% BSA was added, following overnight primary antibody incubation under 4°C. On the next day, peroxidase-coupled rabbit secondary antibody (Affinity) was added to incubate protein bands, which were visualized with enhanced chemiluminescence reagents and quantified with ImageJ.

2.11. Construction and transfection of adenovirus

TGFBR1 recombinant human adenovirus (Ad-TGFBR1) together with its corresponding negative control adenovirus with GFP fluorescence were prepared in Vigene Biosciences (Shandong, China). When CFs grew to about 50% of density, the adenovirus (multiplicity of infection (MOI), 100) was infected in the serum-free medium. At 4 h later, DMEM that contained 10% FBS was added to replace CFs medium. After 48-h incubation, cells were treated with TGF-β1 or Rg3 according to different grouping.

2.12. Statistical analysis

Results were represented by mean ± SD. SPSS21.0 (IBM Corporation, Armonk, NY, USA) was employed for data analysis. Multiple groups were compared by one-way ANOVA, while Student's t-test was performed to examine the difference between the two groups. Difference of $p < 0.05$ stood for statistical significance.

3. Results

3.1. Rg3 improved cardiac function and myocardial fibrosis after infarction

For investigating Rg3's protection against ventricular dysfunction and myocardial fibrosis after MI, a MI model was constructed by permanently ligating LAD coronary artery. HE staining (Fig. 1A) displayed that the cardiomyocytes were arranged neatly in the sham group, but disorderly arranged in MI mice, accompanied by severe necrosis and inflammatory cell infiltration in the ischemic myocardium. However, Rg3 or cap treatment attenuated these pathological alterations. Collagen sedimentation represents a major marker for myocardial fibrosis. Therefore, the formation of collagen was investigated using Masson staining. According to Fig. 1B and E, collagen volume fraction of model group remarkably elevated, but

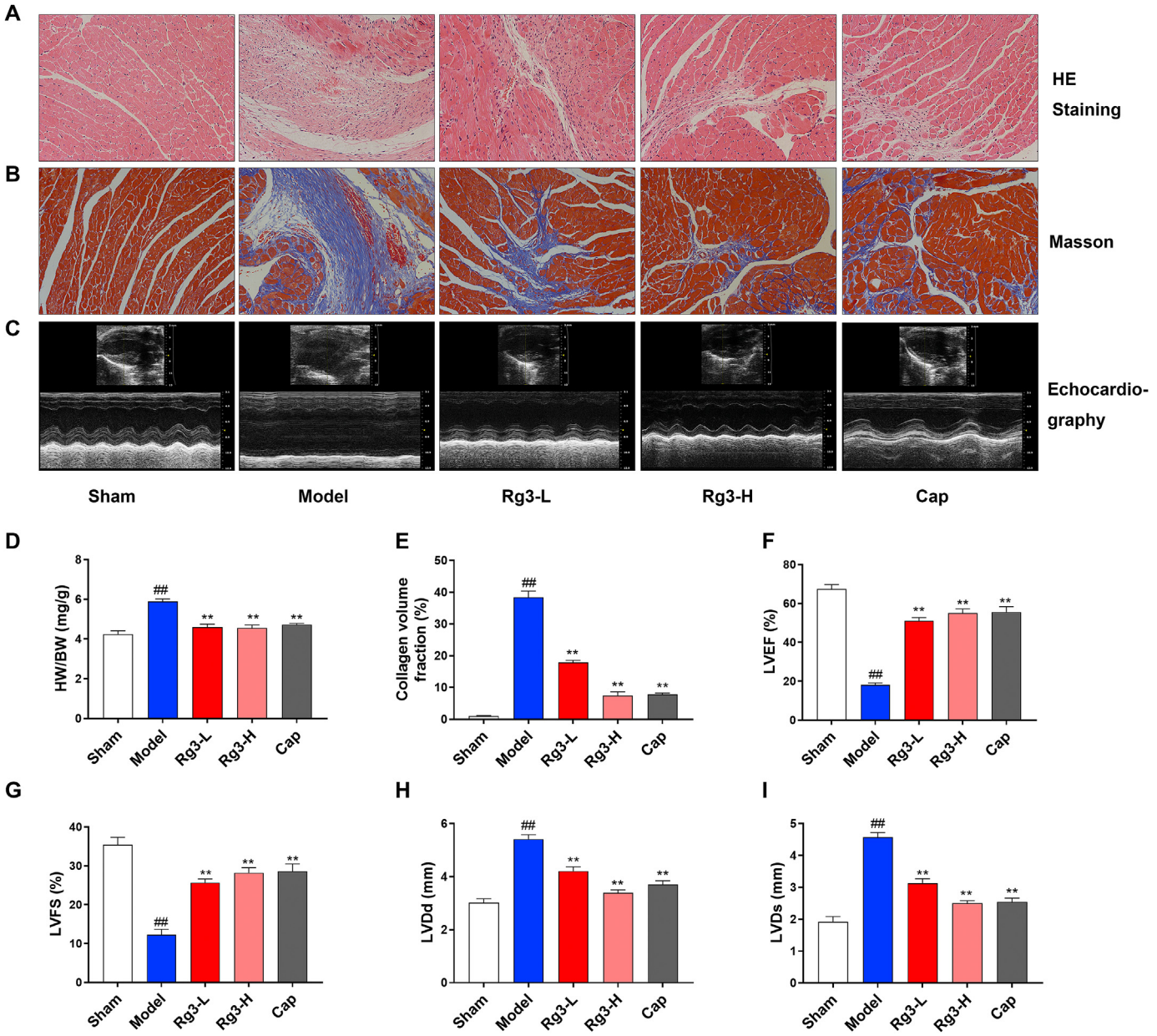

Fig. 1. Rg3 reduces cardiac fibrosis and improves cardiac function post-MI. (A) Typical HE staining images (magnification, 200 ×). (B) Typical Masson trichrome staining images (magnification, 200 ×). The blue area represents collagen sediment. (C) Typical echocardiography images. (D) HW/BW ratio. (E) Collagen volume fraction. (F-I) LVEF, LVFS, LVDd, and LVDs were measured by echocardiography. Results are represented by mean ± SD of at least 3 groups. #$p < 0.05$, ##$p < 0.01$, vs. sham group. *$p < 0.05$, **$p < 0.01$, vs. model group.

collagen deposition was reduced by Rg3 or cap apparently. Fig. 1C displayed the representative images of echocardiography. It was observed that model group showed significantly decreased LVEF and LVFS, while elevated LVDd and LVDs, all of which implied the occurrence of cardiac dysfunction after infarction. In contrast, Rg3 improved cardiac dysfunction dose-dependently (Fig. 1F–I). Moreover, as shown in Fig. 1D, the heart weight to body weight (HW/BW) ratio of model group remarkably elevated relative to sham group, and it was markedly decreased after Rg3 or cap treatment. Collectively, Rg3 improved cardiac function and inhibited collagen deposition after MI.

3.2. Rg3 reduced TGFBR1 signaling pathway related protein levels after infarction by directly targeting TGFBR1

The TGFBR1 pathway has been found to be tightly associated with myocardial fibrosis progression after infarction. However, it remains unclear whether Rg3 exerts cardiovascular protective effects by targeting TGFBR1. In this study, SPRi was conducted with an aim of assessing the Rg3-TGFBR1 binding mechanism. SPRi analysis showed that Rg3 bound rapidly to the TGFBR1 recombinant protein, and its value of equilibrium dissociation constant (K_D) was calculated to be 1.78×10^{-7} M, indicating a good binding affinity (Fig. 2A). Then WB was adopted for detecting TGFBR1 signaling

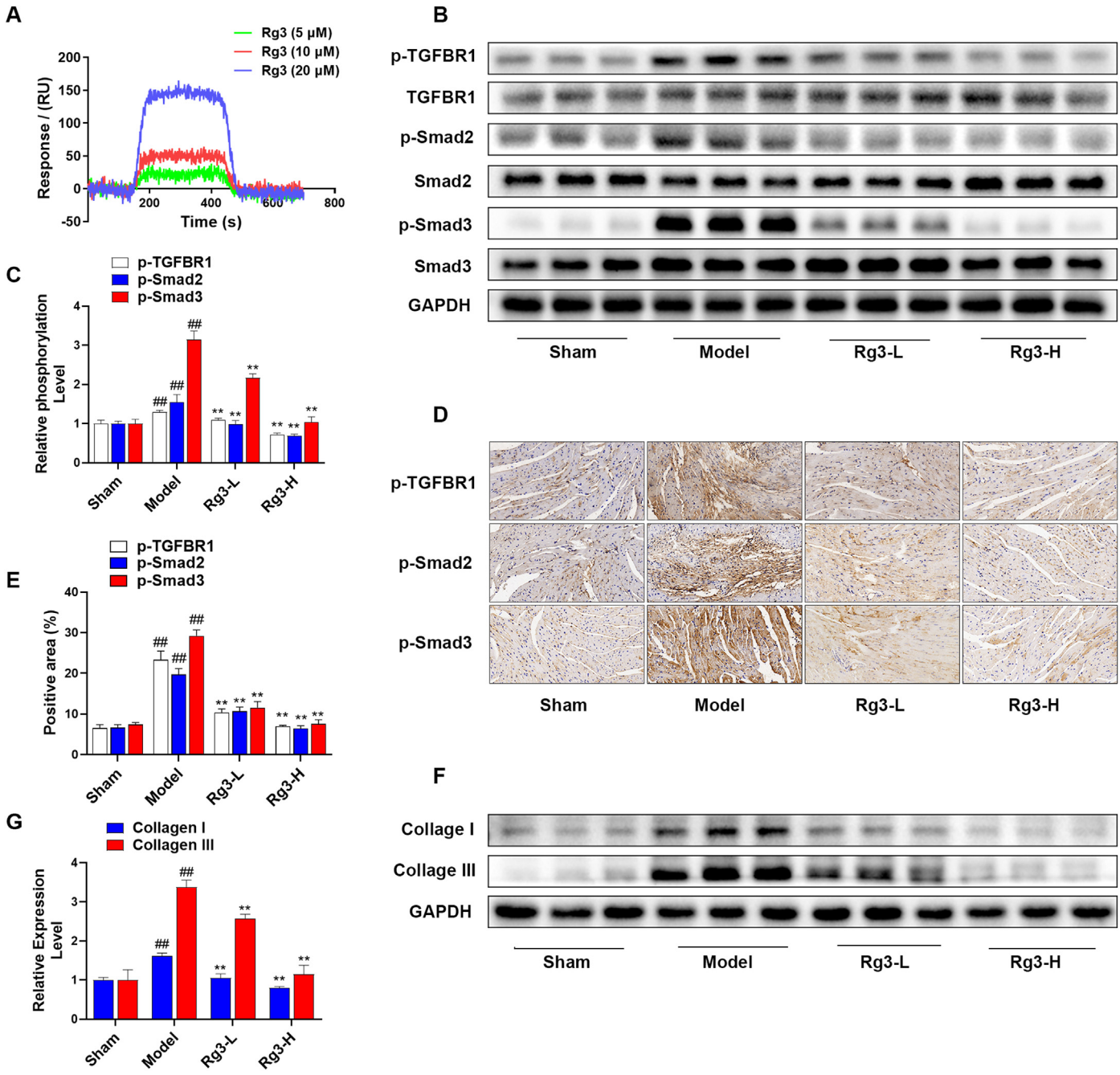

Fig. 2. Rg3 attenuates TGFBR1 signaling pathway related protein levels post-infarction by directly targeting TGFBR1. (A) SPRi fitted curve of Rg3 (5, 10, 20 μM) bound to the TGFBR1 recombinant protein. (B) TGFBR1 pathway-related protein levels within myocardial tissues detected by WB assay. (C) Relative p-TGFBR1, p-Smad2, and p-Smad3 levels were standardized for their respective total proteins. (D) p-TGFBR1, p-Smad3, and p-Smad2 levels within myocardial tissues detected by IHC analysis and their respective quantitative analysis of IHC staining (E). (F) The collagen I and collagen III levels were measured by WB assay, and protein density analysis was normalized to GAPDH (G). Results are represented by mean ± SD of at least 3 groups. #$p < 0.05$, ##$p < 0.01$, vs. sham group. *$p < 0.05$, **$p < 0.01$, vs. model group.

activation, and displayed that TGFBR1, Smad2, and Smad3 phosphorylation levels remarkably increased after infarction, while Rg3 dramatically reduced the elevated expression (Fig. 2B–C). In addition, IHC analysis demonstrated that Rg3 dose-dependently alleviated p-TGFBR1, p-Smad2 and p-Smad3 levels within infarcted myocardium (Fig. 2D–E). Collagen, as the major component of ECM, is significantly up-regulated to restore myocardial structure post-MI. Nevertheless, excessive collagen sedimentation can cause adverse ventricular remodeling and impair cardiac function. Therefore, this work employed WB assay for detecting how Rg3 affected collagen I and collagen III levels. As shown in Fig. 2F–G, model group had markedly up-regulated collagen levels relative to control mice, whereas Rg3 administration remarkably suppressed the up-regulation.

3.3. *Myocardial Tgfbr1 deletion reversed Rg3's suppression on TGFBR1 pathway-related protein levels*

For investigating how TGFBR1 affected Rg3's inhibition of Smad2/Smad3 and collagen-related proteins activation *in vivo*, the

myocardial *Tgfbr1*-deficient mice (*Tgfbr1*$^{\Delta MCK}$) were constructed by crossing MCK-Cre mice with *Tgfbr1*$^{flox/flox}$ mice (Fig. 3A). LoxP sites flanking exon 3 in TGFBR1 gene were contained in *Tgfbr1*$^{flox/flox}$ mice, of which the deletion by Cre/loxP recombination generated a null allele [23]. As shown in Fig. 3B–C, TGFBR1 was not detectable in myocardial tissue of *Tgfbr1*$^{\Delta MCK}$ mice. According to WB assay, compared with *Tgfbr1*$^{flox/flox}$ mice, *Tgfbr1*$^{\Delta MCK}$ mice partly abolished Rg3's inhibition on p-Smad2 and p-Smad3 expression (Fig. 3D–F). IHC analysis of p-Smad2 and p-Smad3 protein came to similar results to WB assay (Fig. 3G–I). In addition, WB assay displayed that the inhibition of Rg3 on collagen I and collagen III was partially abolished by *Tgfbr1* knockdown (Fig. 3J-L). These results indicated that deletion of myocardial *Tgfbr1*, at least in part, abrogated the inhibition of Rg3 on TGFBR1 signaling and collagen deposition.

3.4. Myocardial Tgfbr1 deficiency counteracted the protective effects of Rg3 on cardiac dysfunction and myocardial fibrosis

According to previous description, Rg3's inhibition on Smad2/3 as well as collagen-associated protein levels was dependent on TGFBR1. To further elucidate the role of TGFBR1 in mediating Rg3's therapeutic efficacy in cardiac dysfunction and myocardial fibrosis post-infarction, differences between *Tgfbr1*$^{\Delta MCK}$ mice and *Tgfbr1*$^{flox/flox}$ mice were evaluated. HE staining demonstrated that compared with *Tgfbr1*$^{flox/flox}$ mice receiving LAD coronary artery ligation, necrosis and inflammatory cell infiltration in myocardial tissue were reduced in *Tgfbr1*$^{\Delta MCK}$ infarcted mice. However, Rg3 administration failed to further attenuate these pathological changes after *Tgfbr1* knockdown (Fig. 4A). Masson staining revealed that collagen deposition was alleviated in *Tgfbr1*$^{\Delta MCK}$ MI mice, while the inhibition of Rg3 on cardiac fibrosis was partially abolished after *Tgfbr1* deletion (Fig. 4B and E). Moreover, echocardiography was performed to measure cardiac functions in *Tgfbr1*$^{\Delta MCK}$ mice and *Tgfbr1*$^{flox/flox}$ mice. As shown in Fig. 4C and 4F-I, myocardial *Tgfbr1* deletion partially counteracted the ameliorative effect of Rg3 on cardiac function post-MI, accompanied by HW/BW ratio (Fig. 4D). Based on these results, Rg3's protective effect against cardiac fibrosis and cardiac function was dependent on TGFBR1.

3.5. Rg3 inhibited TGF-β1-induced CFs proliferation together with collagen synthesis by TGFBR1 pathway

Rg3's role in TGF-β1-induced CFs proliferation was analyzed by CCK8 and Edu assays. CCK8 results indicated that Rg3 treatment (5, 10, 20 μM) dose-dependently inhibited TGF-β1-induced CFs proliferation, without inducing any cytotoxicity at concentrations up to 20 μM (Fig. 5A–B). Edu staining suggested that TGF-β1 stimulation increased the red fluorescence of CFs in comparison with control group. However, Rg3 treatment decreased up-regulated Edu-positive cells in a dose-dependent manner (Fig. 5C–D). PCNA has been extensively identified as the proliferation marker related to DNA replication [24]. Besides, Cyclin D1 and CDK6 are key regulators that promote G1-to-S phase progression of cell cycle, which can induce cell proliferation [22,25]. Our study further examined whether Rg3 affected the proliferation through inhibiting cell cycle-associated protein levels. As shown in Fig. 5E–F, PCNA, CDK6, and Cyclin D1 levels markedly increased following TGF-β1 treatment, whereas Rg3 dose-dependently attenuated their increased expression. In addition, gradient concentrations of Rg3 dramatically mitigated TGF-β1-mediated collagen up-regulation dose-dependently (Fig. 5G–H). Later, whether Rg3 inhibited TGFBR1 pathway was investigated. According to Fig. 5I–J, TGF-β1 enhanced TGFBR1 phosphorylation as well as the corresponding downstream molecules. However, Rg3 apparently suppressed TGF-β1-activated TGFBR1, Smad2 and Smad3 phosphorylation dose-dependently, without alteration of the total proteins. These results suggested that Rg3 inhibited CFs proliferation together with collagen synthesis through suppressing TGFBR1/Smads pathway activation.

3.6. TGFBR1 up-regulation partly relieved Rg3's inhibition on CFs growth, collagen synthesis, along with Smads activation

To demonstrate that Rg3's roles in CFs growth, collagen as well as Smads inhibition were mainly attributed to the inhibition of TGFBR1 activity, this work employed recombinant adenovirus overexpressing TGFBR1 (Ad-TGFBR1) together with the corresponding control adenovirus. As shown in Fig. 6A–B, Ad-TGFBR1 transfection dramatically increased Edu-positive cell number (red fluorescence), while TGFBR1 overexpression partially reversed the inhibitory effect of Rg3 on DNA replication. Cell cycle-associated proteins also exhibited similar expression trends. Specifically, TGFBR1 up-regulation remarkably abolished the attenuating effects of Rg3 on PCNA, CDK6 and Cyclin D1 induced by TGF-β1 (Fig. 6C and 6E-G). Besides, it was found that transfection with Ad-TGFBR1 significantly promoted the TGF-β1-induced collagen synthesis, while attenuated Rg3's inhibition on collagen deposition (Fig. 6C and 6H-I). Moreover, p-TGFBR1, p-Smad2, and p-Smad3 levels were more apparently up-regulated following Ad-TGFBR1 transfection, whereas Ad-TGFBR1 transfected CFs showed reversed Rg3-induced inhibition of Smad2 and Smad3 phosphorylation (Fig. 6D and 6J-L). These results suggested that Rg3's inhibitory effect on fibrosis proliferation and collagen synthesis was partially depended on TGFBR1 pathway.

4. Discussion

Myocardial fibrosis is characterized by massive production of extracellular collagen and ECM in the myocardium in response to various pathophysiological stimuli, which is a common pathophysiological phenomenon in different myocardial diseases [3]. Studies have shown that the pathogenesis of myocardial fibrosis post-MI is closely related to various aspects [26,27], including ECM is excessively accumulated due to the imbalance of ECM synthesis and degradation; ROS and DAMPs released by ischemic-hypoxic myocardium trigger inflammatory responses and release a large number of profibrotic factors such as growth factors, cytokines, and chemokines; multiple cell types, like fibroblasts, immune cells and vascular cells also acquire a fibro-genic phenotype under stressful conditions and transform into myofibroblasts. Notably, activated fibroblasts have been identified as critical cell effectors for myocardial fibrosis, which are the main source of collagen and ECM. Although fibroblasts have critical effects on reparative fibrosis, fibrotic alterations disrupt systolic and diastolic functions and cause arrhythmia, ultimately leading to maladaptive remodeling and HF [28]. Current treatments for HF only improve symptoms or cardiac function, but not reverse or delay myocardial fibrosis [29,30]. In this regard, it is urgently needed to develop novel therapeutic agents targeting fibrosis in patients with myocardial disease.

Panax ginseng is a well-known araliaceae plant, and its roots are widely used in Korea, Japan and China for treating diverse disorders like CVDs [31], inflammatory or autoimmune disorder [32,33], and cancer [34]. Ginsenosides, the main bioactive ingredients of its pharmacological effects, are classified into three types [35]: oleanolic acid (Ro), panaxadiol (Rb1, Rb2, Rb3, Rc, Rd, Rg3, Rh2), and panaxatriol (Re, Rg1, Rg2, Rh1). Notably, Rg3, which is a panaxadiol of *panax ginseng*, has cardiovascular protective effects such as anti-cardiac hypertrophy, anti-cardiac failure, and anti-apoptotic activity. Additionally, TGF-β1-stimulated primary CFs and LAD coronary ligation-induced myocardial fibrosis have been recognized as the

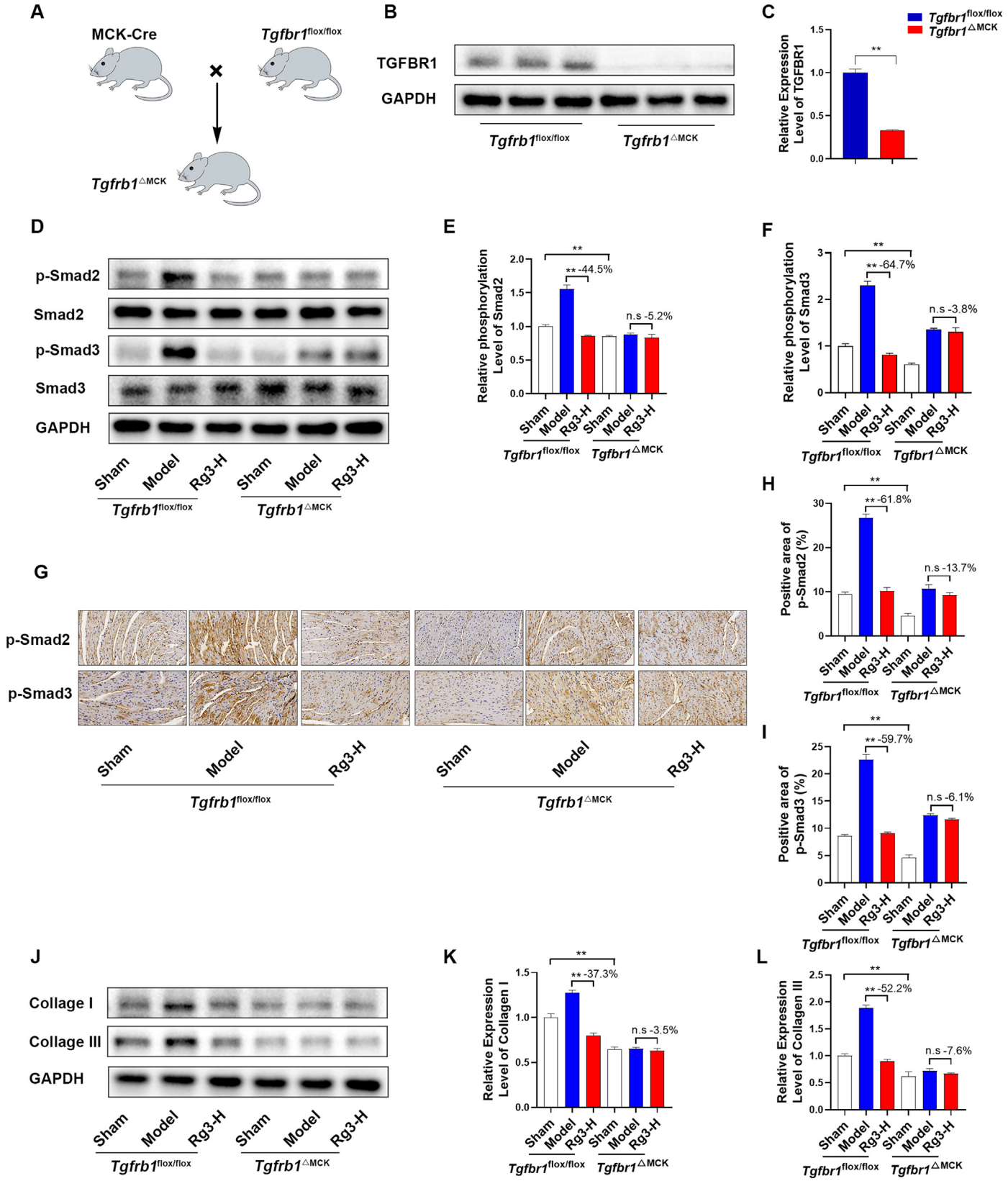

Fig. 3. Myocardial *Tgfbr1* deletion abrogates the inhibition of Rg3 on TGFBR1 signaling and collagen deposition. (A) Schematic diagram showing Cre-MCK mice crossing with *Tgfbr1*$^{flox/flox}$ to generate *Tgfbr1*$^{\Delta MCK}$ mice. (B) WB assay conducted for detection of TGFBR1 level in myocardial tissue and quantitative analysis of TGFBR1/GAPDH (C). (D) WB assay conducted for detection of cardiac Smads expression in *Tgfbr1*$^{flox/flox}$ and *Tgfbr1*$^{\Delta MCK}$ mice. (E) p-Smad2 and p-Smad3 (F) standardized to Smad2 and Smad3, separately. (G) IHC analysis on p-Smad2 and p-Smad3 expression within *Tgfbr1*$^{flox/flox}$ and *Tgfbr1*$^{\Delta MCK}$ mice, and their respective quantitative analysis results (H, I). (J) WB assay carried out for detecting collagen I and collagen III levels, and their protein density analysis was normalized to GAPDH (K, L). Data are represented by mean ± SD from at least 3 groups. *$p < 0.05$, **$p < 0.01$. n.s, not significant.

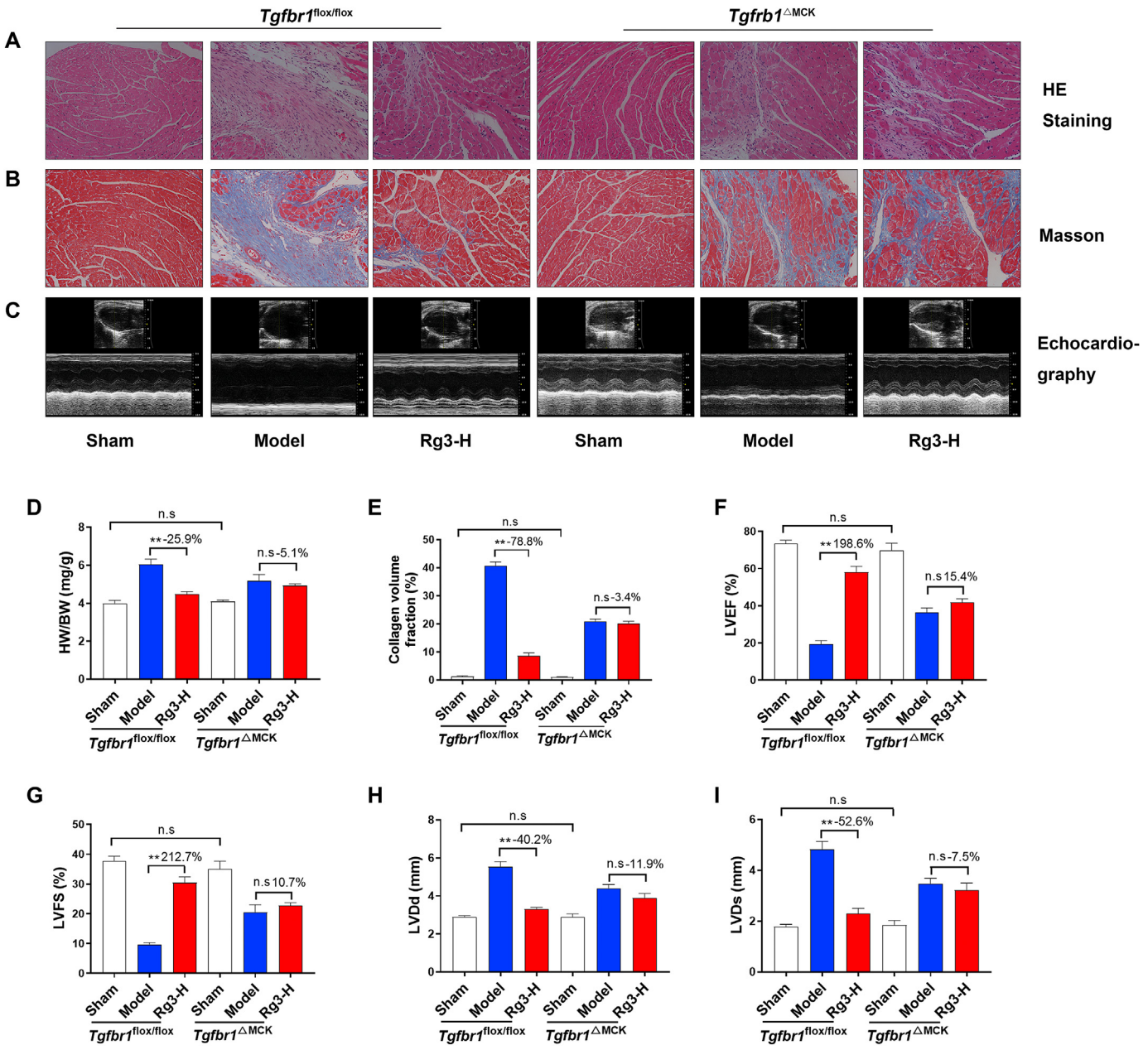

Fig. 4. Myocardial *Tgfbr1* deletion counteracts the protective effect of Rg3 on adverse ventricular remodeling post-MI. (A) Typical HE staining images in *Tgfbr1*$^{\Delta MCK}$ mice and *Tgfbr1*$^{flox/flox}$ mice (magnification, 200 ×). (B) Typical Masson trichrome staining images, of which the blue area represents collagen deposition (magnification, 200 ×). (C) Typical echocardiography images. (D) HW/BW ratio. (E) Fraction of collagen volume. (F-I) LVEF, LVFS, LVDd, and LVDs measured through echocardiography. Data are represented by mean ± SD for at least 3 groups. *$p < 0.05$, **$p < 0.01$. n.s, not significant.

classical models to study the mechanisms and therapeutic agents of myocardial fibrosis *in vitro* and *in vivo*. Therefore, in the present study, myocardial fibrosis post-MI mice were constructed by the ligation of LAD coronary artery. It was found that Rg3 dose-dependently ameliorated cardiac hypertrophy and collagen sediment and improved cardiac dysfunction markedly, consistent with previous results [13]. Moreover, TGF-β1-stimulated primary CFs were adopted to investigate the antifibrotic effect of Rg3 *in vitro*. Consequently, TGF-β1-induced CFs proliferation and up-regulation of cell cycle regulators and collagen deposition were reduced by Rg3 treatment. Interestingly, Rg3 was also related to the proliferation and collagen synthesis of human keloid fibroblasts [36].

TGF-β pathway has an important effect on developing myocardial fibrosis. Currently, the human TGF-β family of multifunctional cytokines contains 3 isoforms, namely, TGF-β1/β2/β3. Among them, TGF-β1 shows close relation with myocardial ischemia and ventricular remodeling, which is one of the most important factors promoting myocardial fibrosis [37]. Canonically, TGF-β1 binds to its receptor TGFBR1, and subsequently phosphorylates its downstream signaling molecules Smad2 and Smad3. TGFBR1 activation plays an important role in activating CFs and extra-matrix collagen production. As confirmed in several studies, TGF-β1 and TGFBR1 expression is up-regulated among cases developing left ventricular dysfunction (LVEF ≤ 40%) in comparison with those with left ventricular function preservation (LVEF > 40%) at 4 months after

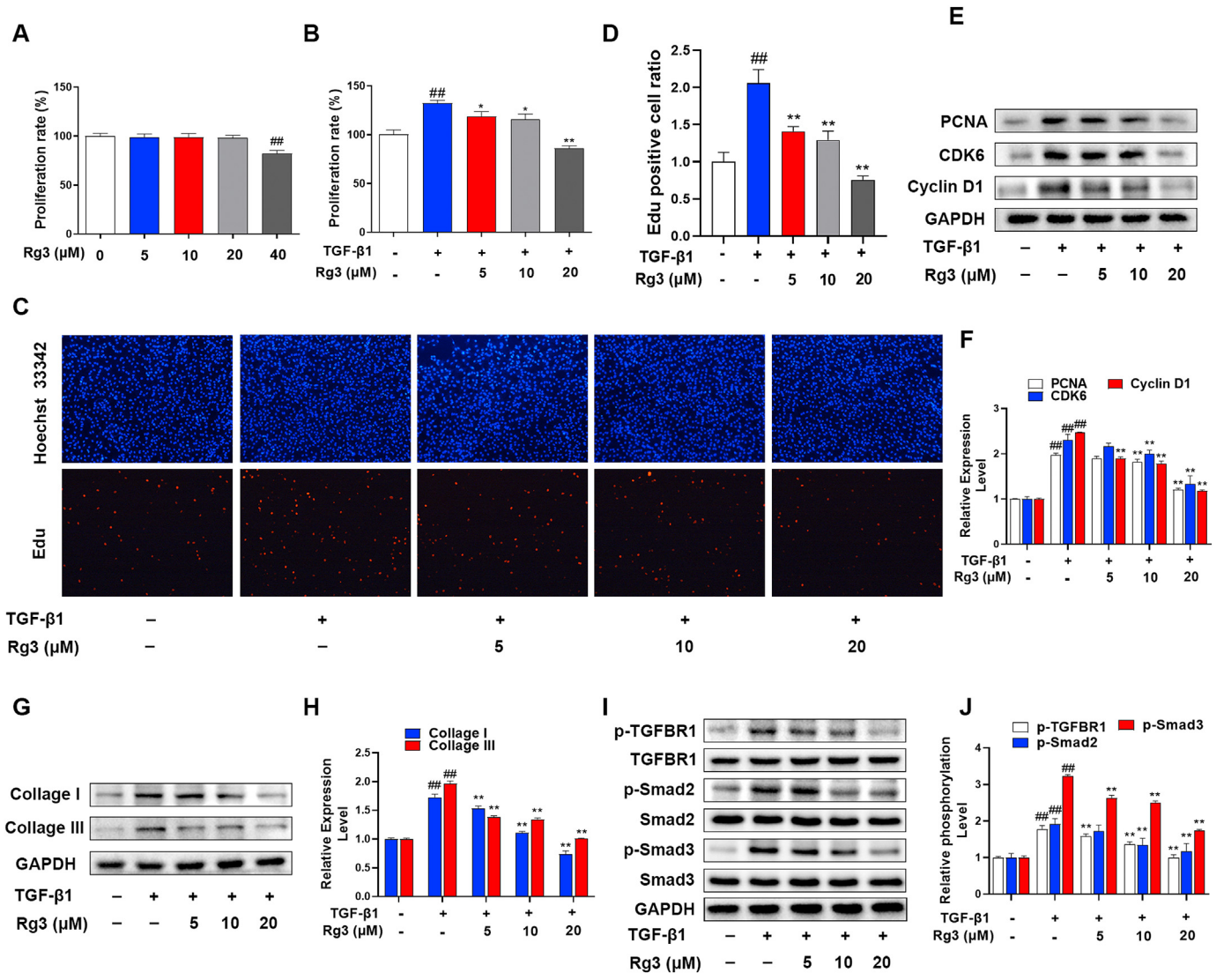

Fig. 5. Rg3 reduces TGF-β1-induced CFs proliferation as well as collagen synthesis through TGFBR1 pathway inactivation. (A) CFs proliferation after incubation with Rg3 at diverse doses (5, 10, 20, 40 μM) was measured by CCK8 assay. (B) CFs were stimulated with TGF-β1 (10 ng/ml), followed by 48-h incubation with/without Rg3 (5, 10, 20 μM), and cell proliferation was measured by CCK8 assay. (C) Typical Edu images showing CFs proliferation (magnification, 200 ×). Red and blue fluorescence stand for proliferating cells and nuclei, separately. (D) Edu-positive cell proportion. (E) CFs were incubated with Rg3 with or without TGF-β1 for a 24-h, and proliferation-associated protein levels were detected by WB assay. (F) Relative expression of PCNA, CDK6, and Cyclin D1 standardized to GAPDH. (G) WB detection of collagen I and collagen III in CFs and their respective quantitative analysis normalized to GAPDH (H). (I) p-TGFBR1, p-Smad3, and p-Smad2 levels and their protein density analysis (J). Results are represented by mean ± SD of at least 3 groups. #$p < 0.05$, ##$p < 0.01$, vs. control group. *$p < 0.05$, **$p < 0.01$, vs. TGF-β1 group.

reperfusion treatment for MI [38,39], which suggest that TGF-β1 and TGFBR1 are the important predictors for left ventricular dysfunction post-MI. Besides, SB-431542, a competitive TGFBR1 blocker, is found to enhance contractility performance and down-regulate extracellular collagen generation under overload pressure [40]. However, due to the poor water solubility and bioavailability, its application has been extremely restricted [41]. Therefore, there is no doubt that targeting TGFBR1 is a specific and effective treatment for myocardial fibrosis post-infarction, and we are committed to seeking efficient and hypo-toxic small molecules of TCM targeting TGFBR1 for treatment of myocardial fibrosis after MI.

With the rapid development of advanced bioinformatics analytical methods and proteomics, there is an explosion of data on ligand/receptor interactions. SPRi is a typical optics sensing and high-throughput detection technology, which has a critical function in biomedical detection and can quantitatively explore the kinetic parameters of biomolecular binding processes in a real-time manner based on the changes in optical refractive index [42]. Our study suggested that Rg3 might be the potential inhibitor of TGFBR1. In addition, we conducted investigation regarding Rg3's effect on TGFBR1 pathway *in vivo* comprehensively. As suggested by IHC and WB results, Rg3 remarkably inhibited TGFBR1, Smad2 and Smad3 phosphorylation in ischemic myocardium. Myocardial conditional *Tgfbr1* knockdown was further adopted to validate the role of TGFBR1 pathway in Rg3's antifibrotic effect. In consequence, *Tgfbr1* knockdown counteracted Rg3's inhibition on p-Smad2 and p-Smad3 expression together with collagen generation, accompanied by protection in maladaptive ventricular remodeling. Taken together, the above results demonstrated that Rg3 protected against myocardial maladaptive remodeling through attenuating myocardial fibrosis and cardiac insufficiency via TGFBR1 pathway *in vivo*. Similarly, *in vitro*, Rg3 significantly suppressed TGF-β1-mediated TGFBR1, Smad2 and Smad3 phosphorylation. TGFBR1 adenovirus was then adopted to verify the action of TGFBR1 in the

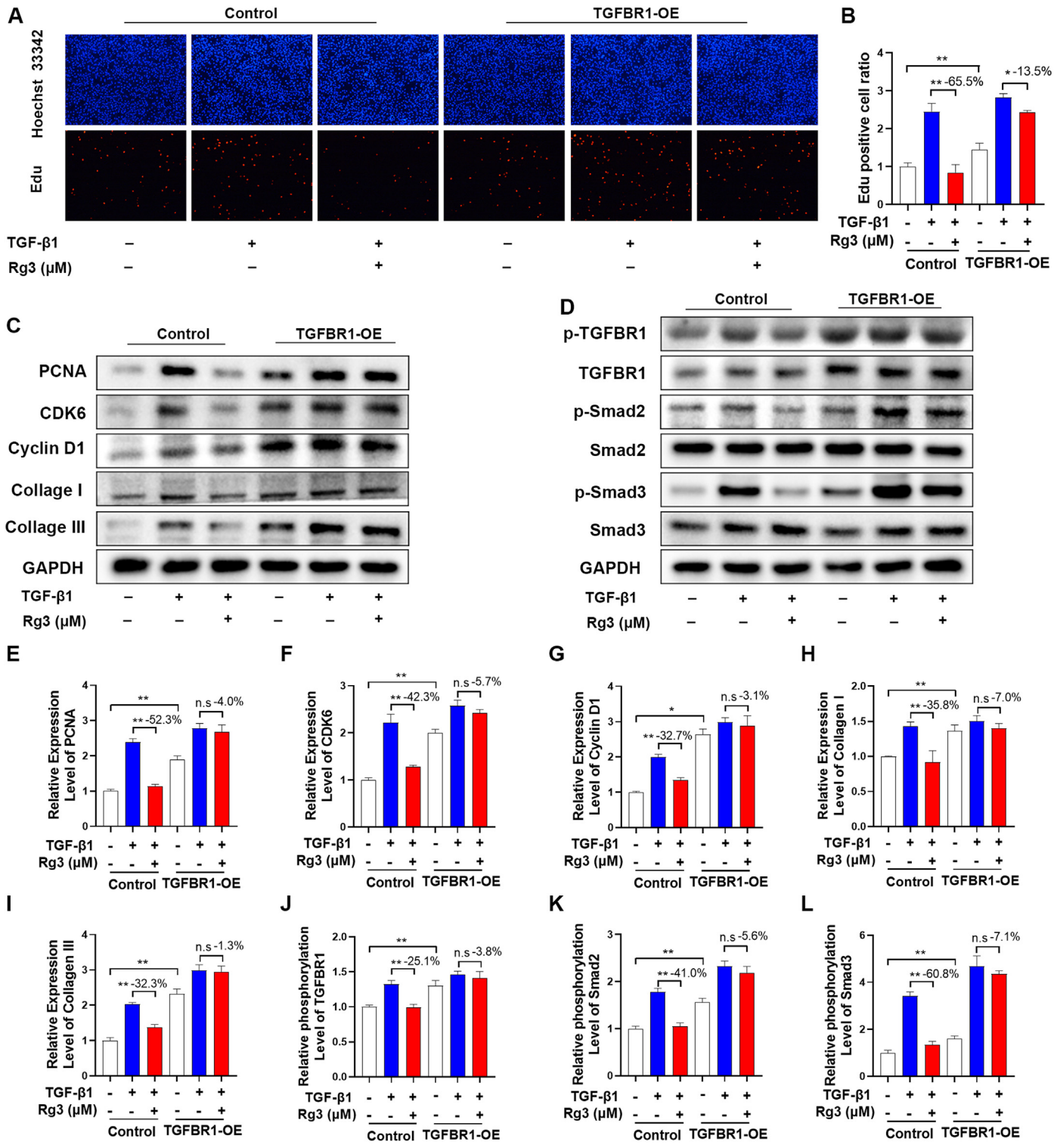

Fig. 6. TGFBR1 overexpression partly abolishes Rg3's inhibition on CFs growth, collagen synthesis, together with Smads activation. (A) CFs were infected with recombinant adenovirus for 48 h, and later stimulated by TGF-β1 (10 ng/ml) and Rg3 (20 μM), and Edu assay was performed to detect CFs proliferation (magnification, 200 ×). Red and blue fluorescence indicate proliferating cells as well as nuclei, separately. (B) Edu-positive cell proportion. (C) Expression of proliferation and collagen-related proteins in CFs following Ad-TGFBR1 or control adenovirus transfection. (D) Protein expression of TGFBR1 signaling in CFs after transfection. Relative PCNA (E), CDK6 (F), Cyclin D1 (G), collagen I (H), collagen III (I), p-TGFBR1 (J), p-Smad2 (K), and p-Smad3 (L) expression. Data are represented by mean ± SD for at least 3 groups. *$p < 0.05$, **$p < 0.01$. n.s, not significant.

pharmacological effect of Rg3. According to our results, TGFBR1 overexpression partially abolished Rg3's inhibition on Smad2/Smad3 activation, CFs growth, together with collagen production, indicating that TGFBR1 was the major pharmacological target of Rg3 for its anti-fibrotic effects *in vitro*. Furthermore, inflammation occurs during the whole cardiac remodeling process post-MI. Consequently, more studies are needed to further investigate Rg3's anti-inflammatory effect post-MI *in vivo* and *in vitro*.

5. Conclusions

In conclusion, this study demonstrates that Rg3 exerts anti-fibrotic effect post-MI by inhibiting CFs proliferation and collagen deposition through TGFBR1 signaling pathways. These results underscore the therapeutic promise of Rg3 in the treatment of cardiac disease, and provides a new perspective on the potential mechanisms of Rg3 against myocardial fibrosis post-MI.

Credit author statement

Honglin Xu: Conceptualization, Investigation, Methodology, Validation, Formal analysis, Writing original draft, Visualization; Haifeng Miao: Investigation, Methodology, Validation, Formal analysis, Visualization; Guanghong Chen: Investigation, Methodology, Validation, Formal analysis; Guoyong Zhang: Investigation, Methodology, Validation, Formal analysis; Yue Hua: Methodology, Validation, Formal analysis; Yuting Wu: Methodology, Validation, Formal analysis; Tong Xu: Methodology, Software, Validation; Xin Han: Methodology, Software, Validation; Changlei Hu: Methodology, Formal analysis; Mingjie Pang: Validation, Formal analysis; Leyi Tan: Data curation, Formal analysis; Bin Liu: Funding acquisition, Methodology, Project administration, Supervision, Validation; Yingchun Zhou: Conceptualization, Funding acquisition, Methodology, Project administration, Supervision, Validation. All authors agree to be accountable for all aspects of work ensuring integrity and accuracy.

Declaration of competing interest

The authors declare that the study was performed without any commercial conflict.

Acknowledgments

This study was supported by the National Natural Science Foundation of China (grant numbers 82274417, 81973645, 81774100), Natural Science Foundation of Guangdong Province (Nos. 2022A1515011630, 2021A1515220010), and Guangdong Basic and Applied Basic Research Foundation (No. 2022A1515110870).

Appendix A. Supplementary data

Supplementary data to this article can be found online at https://doi.org/10.1016/j.jgr.2023.06.007.

References

[1] Tsao CW, Aday AW, Almarzooq ZI, Alonso A, Beaton AZ, Bittencourt MS, et al. Heart disease and stroke statistics-2022 update: a report from the American heart association. Circulation 2022;145:e153–639.
[2] Roth GA, Mensah GA, Johnson CO, Addolorato G, Ammirati E, Baddour LM, et al. Global burden of cardiovascular diseases and risk factors, 1990-2019: update from the GBD 2019 study. J Am Coll Cardiol 2020;76:2982–3021.
[3] Frangogiannis NG. Cardiac fibrosis. Cardiovasc Res 2021;117:1450–88.
[4] Travers JG, Tharp CA, Rubino M, McKinsey TA. Therapeutic targets for cardiac fibrosis: from old school to next-gen. J Clin Invest 2022:132.
[5] Mechesso AF, Quah Y, Park SC. Ginsenoside Rg3 reduces the adhesion, invasion, and intracellular survival of Salmonella enterica serovar Typhimurium. J Ginseng Res 2021;45:75–85.
[6] Huang WC, Huang TH, Yeh KW, Chen YL, Shen SC, Liou CJ. Ginsenoside Rg3 ameliorates allergic airway inflammation and oxidative stress in mice. J Ginseng Res 2021;45:654–64.
[7] Xia J, Ma S, Zhu X, Chen C, Zhang R, Cao Z, et al. Versatile ginsenoside Rg3 liposomes inhibit tumor metastasis by capturing circulating tumor cells and destroying metastatic niches. Sci Adv 2022;8:eabj1262.
[8] Min JK, Kim JH, Cho YL, Maeng YS, Lee SJ, Pyun BJ, et al. 20(S)-Ginsenoside Rg3 prevents endothelial cell apoptosis via inhibition of a mitochondrial caspase pathway. Biochem Biophys Res Commun 2006;349:987–94.
[9] Xu W, Lyu W, Duan C, Ma F, Li X, Li D. Preparation and bioactivity of the rare ginsenosides Rg3 and Rh2: an updated review. Fitoterapia 2023;167:105514.
[10] Fan X, Xu Y, Zhu D, Ji Y. Pharmacokinetic comparison of 20(R)- and 20(S)-Ginsenoside Rh1 and 20(R)- and 20(S)-Ginsenoside Rg3 in rat plasma following oral administration of radix ginseng rubra and sheng-Mai-san extracts. Evid Based Complement Alternat Med 2017;2017:6451963.
[11] Guo M, Guo G, Xiao J, Sheng X, Zhang X, Tie Y, et al. Ginsenoside Rg3 stereoisomers differentially inhibit vascular smooth muscle cell proliferation and migration in diabetic atherosclerosis. J Cell Mol Med 2018;22:3202–14.
[12] Ren B, Feng J, Yang N, Guo Y, Chen C, Qin Q. Ginsenoside Rg3 attenuates angiotensin II-induced myocardial hypertrophy through repressing NLRP3 inflammasome and oxidative stress via modulating SIRT1/NF-κB pathway. Int Immunopharmacol 2021;98:107841.
[13] Lai Q, Liu FM, Rao WL, Yuan GY, Fan ZY, Zhang L, et al. Aminoacylase-1 plays a key role in myocardial fibrosis and the therapeutic effects of 20(S)-ginsenoside Rg3 in mouse heart failure. Acta Pharmacol Sin 2022;43:2003–15.
[14] Hata A, Chen YG. TGF-β signaling from receptors to Smads. Cold Spring Harb Perspect Biol 2016;8.
[15] Hanna A, Frangogiannis NG. The role of the TGF-β superfamily in myocardial infarction. Front Cardiovasc Med 2019;6:140.
[16] Rodon J, Carducci MA, Sepulveda-Sánchez JM, Azaro A, Calvo E, Seoane J, et al. First-in-human dose study of the novel transforming growth factor-β receptor I kinase inhibitor LY2157299 monohydrate in patients with advanced cancer and glioma. Clin Cancer Res 2015;21:553–60.
[17] Santini V, Valcárcel D, Platzbecker U, Komrokji RS, Cleverly AL, Lahn MM, et al. Phase II study of the ALK5 inhibitor galunisertib in very low-, low-, and intermediate-risk myelodysplastic syndromes. Clin Cancer Res 2019;25:6976–85.
[18] Xie SS, Dong ZH, He Y, Chen ZW, Yang Q, Ma WX, et al. Cpd-0225 attenuates renal fibrosis via inhibiting ALK5. Biochem Pharmacol 2022;204:115240.
[19] Cheng LQ, Na JR, Bang MH, Kim MK, Yang DC. Conversion of major ginsenoside Rb1 to 20(S)-ginsenoside Rg3 by microbacterium sp. GS514. Phytochemistry 2008;69:218–24.
[20] Tan Z, Jiang X, Zhou W, Deng B, Cai M, Deng S, et al. Taohong siwu decoction attenuates myocardial fibrosis by inhibiting fibrosis proliferation and collagen deposition via TGFBR1 signaling pathway. J Ethnopharmacol 2021;270:113838.
[21] Xu H, Liu M, Chen G, Wu Y, Xie L, Han X, et al. Anti-inflammatory effects of ginsenoside Rb3 in LPS-induced macrophages through direct inhibition of TLR4 signaling pathway. Front Pharmacol 2022;13:714554.
[22] Romero-Pozuelo J, Figlia G, Kaya O, Martin-Villalba A, Teleman AA. Cdk4 and Cdk6 couple the cell-cycle machinery to cell growth via mTORC1. Cell Rep 2020;31:107504.
[23] Larsson J, Goumans MJ, Sjöstrand LJ, van Rooijen MA, Ward D, Levéen P, et al. Abnormal angiogenesis but intact hematopoietic potential in TGF-beta type I receptor-deficient mice. Embo J 2001;20:1663–73.
[24] González-Magaña A, Blanco FJ. Human PCNA structure, function and interactions. Biomolecules 2020;10.
[25] Pestell RG. New roles of cyclin D1. Am J Pathol 2013;183:3–9.
[26] Aujla PK, Kassiri Z. Diverse origins and activation of fibroblasts in cardiac fibrosis. Cell Signal 2021;78:109869.
[27] Zhang Q, Wang L, Wang S, Cheng H, Xu L, Pei G, et al. Signaling pathways and targeted therapy for myocardial infarction. Signal Transduct Target Ther 2022;7:78.
[28] González A, Schelbert EB, Díez J, Butler J. Myocardial interstitial fibrosis in heart failure: biological and translational perspectives. J Am Coll Cardiol 2018;71:1696–706.
[29] López B, Ravassa S, Moreno MU, José GS, Beaumont J, González A, et al. Diffuse myocardial fibrosis: mechanisms, diagnosis and therapeutic approaches. Nat Rev Cardiol 2021;18:479–98.
[30] Czubryt MP, Hale TM. Cardiac fibrosis: pathobiology and therapeutic targets. Cell Signal 2021;85:110066.
[31] Hyun SH, Bhilare KD, Park C-K, Kim J-H. Effects of Panax ginseng and ginsenosides on oxidative stress and cardiovascular diseases: pharmacological and therapeutic roles. Journal of Ginseng Research 2022;46:33–8.
[32] Yang S, Li F, Lu S, Ren L, Bian S, Liu M, et al. Ginseng root extract attenuates inflammation by inhibiting the MAPK/NF-κB signaling pathway and activating autophagy and p62-Nrf2-Keap1 signaling *in vitro* and *in vivo*. Journal of Ethnopharmacology 2022;283:114739.
[33] Xu HL, Chen GH, Wu YT, Xie LP, Tan ZB, Liu B, et al. Ginsenoside Ro, an oleanolic saponin of Panax ginseng, exerts anti-inflammatory effect by direct inhibiting toll like receptor 4 signaling pathway. J Ginseng Res 2022;46:156–66.
[34] Hwang S-K, Jeong Y-J, Cho H-J, Park Y-Y, Song K-H, Chang Y-C. Rg3-enriched red ginseng extract promotes lung cancer cell apoptosis and mitophagy by ROS production. Journal of Ginseng Research 2022;46:138–46.
[35] Kim S-J, Murthy HN, Hahn E-J, Lee HL, Paek K-Y. Parameters affecting the extraction of ginsenosides from the adventitious roots of ginseng (Panax ginseng C.A. Meyer). Separation and Purification Technology 2007;56:401–6.
[36] Tang M, Bian W, Cheng L, Zhang L, Jin R, Wang W, et al. Ginsenoside Rg3 inhibits keloid fibroblast proliferation, angiogenesis and collagen synthesis *in vitro* via the TGF-β/Smad and ERK signaling pathways. Int J Mol Med 2018;41:1487–99.

[37] Hu H-H, Chen D-Q, Wang Y-N, Feng Y-L, Cao G, Vaziri ND, et al. New insights into TGF-β/Smad signaling in tissue fibrosis. Chemico-Biological Interactions 2018;292:76–83.
[38] Devaux Y, Bousquenaud M, Rodius S, Marie P-Y, Maskali F, Zhang L, et al. Transforming growth factor β receptor 1 is a new candidate prognostic biomarker after acute myocardial infarction. BMC Medical Genomics 2011;4:83.
[39] Boileau A, Lalem T, Vausort M, Zhang L, Devaux Y. A 3-gene panel improves the prediction of left ventricular dysfunction after acute myocardial infarction. International Journal of Cardiology 2018;254:28–35.
[40] Nunez-Toldra R, Kirwin T, Ferraro E, Pitoulis FG, Nicastro L, Bardi I, et al. Mechanosensitive molecular mechanisms of myocardial fibrosis in living myocardial slices. ESC Heart Fail 2022;9:1400–12.
[41] Zhang J, Li R, Liu Q, Zhou J, Huang H, Huang Y, et al. SB431542-Loaded liposomes alleviate liver fibrosis by suppressing TGF-β signaling. Mol Pharm 2020;17:4152–62.
[42] Bocková M, Slabý J, Špringer T, Homola J. Advances in surface plasmon resonance imaging and microscopy and their biological applications. Annu Rev Anal Chem (Palo Alto Calif) 2019;12:151–76.